

**UCC Library and UCC researchers have made this item openly available.
 Please [let us know](#) how this has helped you. Thanks!**

Title	Synchrotron x-ray fluorescence analysis reveals diagenetic alteration of fossil melanosome trace metal chemistry
Author(s)	Rogers, Christopher S.; Webb, Samuel M.; McNamara, Maria E.
Publication date	2021-10-20
Original citation	Rogers, C. S., Webb, S. M. and McNamara, M. E. (2021) 'Synchrotron x-ray fluorescence analysis reveals diagenetic alteration of fossil melanosome trace metal chemistry', <i>Palaeontology</i> , 64(1), pp. 63-73. doi: 10.1098/rspb.2019.1649
Type of publication	Article (peer-reviewed)
Link to publisher's version	https://onlinelibrary.wiley.com/doi/full/10.1111/pala.12506 http://dx.doi.org/10.1098/rspb.2019.1649 Access to the full text of the published version may require a subscription.
Rights	© 2020 The Palaeontological Association. This is the peer reviewed version of the following article: Rogers, C.S., Webb, S.M. and McNamara, M.E. (2021), Synchrotron x-ray fluorescence analysis reveals diagenetic alteration of fossil melanosome trace metal chemistry. <i>Palaeontology</i> , 64: 63-73, which has been published in final form at https://doi.org/10.1111/pala.12506 This article may be used for non-commercial purposes in accordance with Wiley Terms and Conditions for Self-Archiving.
Embargo information	Access to this article is restricted until 12 months after publication by request of the publisher.
Embargo lift date	2021-10-20
Item downloaded from	http://hdl.handle.net/10468/11870

Downloaded on 2021-11-27T15:11:53Z

24 to show that thermal maturation can dramatically alter melanosome trace element chemistry.
25 In particular, maturation of melanosomes in Cu-rich solutions results in significant depletion
26 of Zn, likely due to low pH and competition effects with Cu. These results confirm fossil
27 melanosome chemistry is susceptible to alteration due to variations in local chemical
28 conditions during diagenesis. Maturation experiments can provide essential data on
29 melanosome chemical taphonomy required for accurate interpretations of preserved chemical
30 signatures in fossils.

31

32 **Keywords:** fossil, soft tissue, taphonomy, Synchrotron-X-ray fluorescence.

33

34 MELANIN is an essential biomolecule in animals that supports immunity (Agius and Roberts
35 2003; Nappi and Christensen 2005) and facilitates key physiological processes including
36 directional photoreception in the eye (Oakley *et al.* 2015) and the protection of tissues from
37 UV damage (Brenner and Hearing 2007). Melanin may also contribute to metal homeostasis
38 via its high binding affinity for metal ions such as Ca^{+2} , Fe^{+3} , Cu^{+2} and Zn^{+2} (Hong and
39 Simon 2007; Wogelius *et al.* 2011; Rossi *et al.* 2019) (albeit the two common forms of
40 melanin, eumelanin and pheomelanin, differ in metal affinity) (Wogelius *et al.* 2011,
41 Manning *et al.* 2019). Remarkably, evidence of melanin has been reported from many
42 vertebrate fossils, usually in association with preserved melanosomes (micron-sized
43 organelles) (e.g. Lindgren *et al.* 2012; McNamara *et al.* 2016). As with melanin in extant
44 animals (Hong and Simon, 2007, fossil melanin can associate with metals, especially Cu
45 (Wogelius *et al.* 2011) and Zn (Manning *et al.* 2019). Preserved associations between these
46 metals and melanosomes can be tissue- and taxon-specific (Rogers *et al.* 2019; Rossi *et al.*
47 2019), thus offering the potential to inform on the internal anatomy (Rossi *et al.* 2019) and

48 phylogenetic affinities (Rogers *et al.* 2019) of fossils and the functional evolution of melanin
49 (Rossi *et al.* 2019).

50

51 The metal inventory of fossil melanin, however, differs from that of modern analogues, even
52 in closely related taxa (Rossi *et al.* 2019; Rogers *et al.* 2019). In the case of vertebrate eye
53 melanosomes, concentrations of Zn are markedly lower in fossils relative to modern
54 vertebrate eyes, and concentrations of Cu and Fe are higher (Rogers *et al.* 2019). The origins
55 of these differences are unclear, thus impacting our ability to confidently interpret preserved
56 melanosome chemistry. Previous work on fossils acknowledged the possibility of diagenetic
57 alteration of the trace metal inventory of melanosomes (Wogelius *et al.* 2011); this is
58 supported by experimental evidence that the trace element chemistry of melanin is sensitive
59 to fluctuations in pH (Hong and Simon 2007) and high metal concentrations (Chen *et al.*
60 2009). Characterization of the impact of diagenesis on melanosome trace metal chemistry is
61 therefore essential to identify taphonomic biases in the melanosome fossil record.

62

63 Here, we resolved these issues by conducting maturation experiments on melanosomes from
64 extant vertebrate eyes at elevated pressures and/or temperatures and with different chemical
65 media in order to simulate how different pore fluids (i.e. sources of metal ions) interact with
66 melanosomes during diagenesis. Analysis of the results using synchrotron rapid scan-X-ray
67 fluorescence analysis (SRS-XRF) and X-ray absorption spectroscopy (XAS) reveals which
68 melanosome-associated elements are susceptible to changes in concentration during
69 diagenesis. Critically, the experimental data aid interpretations of the chemical differences
70 between fossil and modern eye melanosomes, thus informing on key biases in the
71 melanosome fossil record.

72

73 **MATERIALS and METHODS**

74 *Modern specimens*

75 Specimens of European sea bass (*Dicentrarchus labrax* n = 14) were obtained from
76 commercial suppliers and dissected within 24 h after death. One eye from each animal was
77 bisected and melanin was enzymatically extracted from the posterior half of each eye
78 (including the melanosome-rich choroid and retinal pigment epithelium (RPE)) using the
79 method in Rossi *et al.* (2019). The extraction process breaks down cellular material and can
80 degrade phaeomelanin, yielding extracts that are biased towards eumelanin (Liu et al. 2005).

81

82 *Fossil specimens*

83 Preserved melanosomes from the eyespot of a specimen of *Dapalis macrurus* (CKGM F 6
84 427; Actinopterygii: Perciformes, from Alpes de Haute-Provence, France (Oligocene)) and
85 eyespots from the fossil teleosts Tetradontiformes indet. (NHMD 199 838; from the Fur
86 Formation, Denmark (Eocene)) and *Knightia* (FOBU 17 591; Actinopterygii: Clupeiformes
87 from the Fossil Butte member of the Green River formation, Colorado/Utah/Wyoming
88 (Eocene)) were reported in Rogers *et al.* (2019) and analyzed further as below.

89

90 The respective fossil localities vary in lithology and diagenetic history. NHMD 199 838 is
91 hosted in diatomite that was deposited in a restricted marine basin (Pedersen and Buchardt,
92 1996) and experienced at least 40–45°C and ~33–49 bar during diagenesis (McNamara et al.
93 2013). FOBU 17 591 is hosted in laminated limestone that was deposited in a restricted
94 terrestrial basin with marked salinity fluctuations during deposition (Loewen and Buchheim
95 1998). Data on diagenetic history are not available for the Fossil Butte Member (part of the
96 Fossil Basin); sediments from the Uinta Basin of the Green River Formation experienced

97 burial conditions of up to 65–180°C and ~400–2000 bar (McNamara et al. 2013). CKGM F
98 6427 is preserved in a laminated limestone but lacks stratigraphic data; specimens of this
99 taxon are common in the freshwater/brackish lacustrine limestones of the Campagne-Calavon
100 Formation of Alpes de Haute-Provence (Gaudant, 2015), though data on burial history are not
101 available.

102

103 Institutional abbreviations: NHMD, Natural History Museum of Denmark; CKGM, Cork
104 Geological Museum at University College Cork; FOBU, Fossil Butte National Monument.

105

106 *EDTA treatment of melanin*

107 Unmatured melanin (50–100 mg) extracted from a single *Dicentrarchus* eye was added to an
108 aqueous solution of EDTA (one ml) for 24 h at room temperature and then centrifuged. This
109 process was repeated six times followed by washing four times in biomolecular-grade water
110 in order to remove excess EDTA. The EDTA-treated extract was then added to one ml of 16
111 mmol Cu-solution for 24 h at room temperature before being washed twice in 10⁻³ M HCl to
112 precipitate any Cu still in solution (Hong *et al.* 2004). The extract was washed twice in
113 biomolecular water and once in acetone. Half of the extract was experimentally matured (see
114 below).

115

116 *Experimental maturation*

117 Taphonomic studies investigating the impact of maturation on soft tissues typically use
118 elevated temperatures and pressures for relatively short periods of time (usually < 24 h) to
119 artificially simulate aspects of the maturation process (McNamara *et al.* 2013; Colleary *et al.*
120 2015). Such experiments are known to yield morphological and chemical phenomena similar
121 to those exhibited by fossils (Stankiewicz *et al.* 2000). Melanosome extracts for experimental

122 maturation (n = 12) were each inserted into separate Au capsules. To each capsule was added
123 one ml of experimental medium, defined as follows. The EDTA-treated extract used distilled
124 deionized (DD) water. All other extracts used either DD water, “Cu-solution” (Trace Cert
125 Copper standard for AAS (1 000 mg l⁻¹)), “Zn-solution” (Trace Cert Zinc standard for AAS
126 (1 000 mg l⁻¹)) or “Cu-Zn-solution” (50:50 mixture of Trace Cert Copper and Zinc standards
127 for AAS (Rogers et al. 2020 (Table S1))). The inclusion of metal ion solution in some
128 experiments is designed to test how variation in diagenetic pore fluid chemistry impacts
129 melanin chemistry. All metal ion solutions have a concentration of 16 mmol and are at pH 3.

130

131 Brushes were used to remove any extract or experimental medium from the termini of each
132 capsule prior to them being welded shut with a Lampert PUK 4 microwelding system. Sealed
133 capsules were thermally matured for 24 h at 200°C in either an oven at one bar or, for some
134 samples (including EDTA-treated extracts) a custom-built high-pressure high-temperature rig
135 (StrataTech, UK) at 120 bar. It was not possible to measure the pH of the experimental
136 medium at the end of the experiment due to the small size of the capsules and unpredictable
137 escape of fluid from the capsules upon opening.

138

139 *Synchrotron Rapid Scanning-X-ray Fluorescence (SRS-XRF) analysis*

140 X-ray fluorescence spectra were collected from matured and untreated extracts and fossils at
141 beamline 2-3 at the Stanford Synchrotron Radiation Lightsource (SSRL). Extracts and small
142 samples (ca. one mm²) of dark brown carbonaceous material from the eyespot of the fossil
143 fish *Dapalis macrurus* (Oligocene, CKGM F 6 427) were mounted on kapton tape. Samples
144 were spatially rastered by a microfocused beam of two μm² provided by an Rh-coated
145 Kirkpatrick-Baez mirror pair with 20–50 ms/pixel dwell time. A Si (111) double crystal
146 monochromator was used to set incident X-ray energy at 11 keV; the storage ring was in top-

147 off mode at three GeV and contained 500 mA. Samples were mounted at 45° to the incident
148 X-ray and the intensity of the beam was measured using a nitrogen-filled ion chamber. At
149 each data point, the intensity of fluorescence lines for selected elements (P, S, Ca, Ti, Mn, Fe,
150 Ni, Cu and Zn) was collected and monitored using an Xpress3 pulse processing system
151 (Quantum Detectors) coupled to a silicon drift Vortex detector (Hitachi, USA) for energy
152 discrimination.

153

154 *SRS-XRF data processing*

155 MicroAnalysis Toolkit software (Webb 2011) was used to normalize fluorescence spectra
156 and calibrate concentrations of each element in $\mu\text{g}/\text{cm}^2$ against NIST traceable thin-film
157 elemental standards. Mean concentrations and standard deviation values for each element
158 were calculated for selected regions of interest. Inspection of SRS-XRF spectra from the
159 Multi-Channel Analyzer (MCA) data reveals that in extracts the concentrations of certain
160 elements (P, S, Ti and Mn) are too low to be discriminated confidently from the background
161 (Rogers et al. 2020 (Figs S1–S7)). Concentration data from these elements were therefore
162 excluded from further analyses. Ni was identified in the MCA data but concentrations ($< \text{nine}$
163 $\mu\text{g}/\text{cm}^2$) were markedly lower than those of other elements and thus Ni was also excluded
164 from further analysis.

165

166 The SRS-XRF data were analyzed further using Linear Discriminant Analysis (LDA) in
167 PAST (Hammer *et al.* 2001) to visualize variations in the chemistry of selected elements (Ca,
168 Fe, Cu and Zn) among the melanin extracts and fossil melanosomes. The significance of
169 differences in concentration among samples was assessed using ANOVA or non-parametric
170 alternatives (Kruskal-Wallis and Welch's F-test) and appropriate pairwise post hoc analyses

171 (Tukey, Mann Whitney and Dunn, respectively). Differences in elemental concentrations
172 among extracts were visualized using box plots.

173

174 *X-ray absorption spectroscopy (XAS)*

175 EDTA-treated extracts and samples from the eyespot of *Dapalis* were mapped at beamlines
176 2-3 and 10-2 at the Stanford Synchrotron Radiation Lightsource (SSRL). At beamline 2-3
177 extracts were analyzed as above. At beamline 10-2 extracts were analyzed using a 25–200 μm
178 beam using a series of tungsten apertures. Four to six points of interest were selected from
179 each SRS-XRF map. XAS spectra were collected from these points by driving the emitted
180 intensity from $\sim 8\,787$ eV to $\sim 9\,827$ eV across the Cu K edge (set at 8 987 eV using a Cu foil)
181 in a stepwise fashion (step size of 10 eV from 8 749 to 8 958 eV, except for between 8 959 to
182 9 006 eV (i.e. across the Cu K edge) where step size of 0.35 eV was used. Between two and
183 seven repeat scans (15 min each) were collected at each point.

184

185 A Cu foil was used to calibrate the energy of the monochromator. X-ray absorption near edge
186 structure spectroscopy (XANES) was used to investigate the oxidation state of Cu associated
187 with the melanosomes in our dataset. Each spectrum was monitored for loss of intensity and
188 photo-reduction associated with exposure to the electron beam. No evidence for photo-
189 reduction was observed among replicate scans and repeat scans at each point are mutually
190 consistent. Spectra were processed as standard (i.e. via normalization and background
191 removal) in Athena (Ravel and Newville 2005).

192

193 **RESULTS**

194 *Trace metal concentrations in matured melanosome extracts*

195 Linear Discriminant Analysis (LDA) plots of the SRS-XRF data show extensive overlap of
196 data from unmaturred and maturated melanosomes in chemospace (Fig. 1A–B). Differences in
197 trace element chemistry between untreated extracts and extracts experimentally maturated in
198 DD water are not statistically significant (p -values=0.1034–0.8206, Rogers et al. 2020 (Table
199 S2A–C)); these two samples cannot therefore be distinguished chemically.

200

201 Concentrations of Ca (Welch F: df = 16.18, F = 73.39, $p = 7.91^{-11}$) and Cu (df = 17.47, F =
202 118.8, $p = 5.792^{-13}$) are significantly different between unmaturred extracts and extracts
203 maturated in Cu and/or Zn-solutions (Fig. 2, Rogers et al. 2020 (Table S2A)). More
204 specifically, concentrations of Ca are significantly lower in extracts maturated in Zn-solution
205 and mixed Cu-Zn-solution (Dunn’s post hoc $p = 0.002$ – 0.006). Concentrations of Cu are
206 higher in extracts maturated in Cu-solution and mixed Cu-Zn-solution ($p = 0.001$ – 0.002)
207 (Rogers et al. 2020 (Table S2B–C)). Concentrations of Zn are significantly lower in all
208 extracts maturated with Cu- and/or Zn-solution (Kruskal-Wallis H (χ^2) = 23.33, $p = 0.001$;
209 Dunn’s post hoc $p = 0.001$ – 0.006). Variations in Fe concentrations among untreated and
210 experimentally maturated extracts are not significant (ANOVA df = 2.115, F = 17.5, $p =$
211 0.1034).

212

213 *Comparison with fossil trace element chemistry*

214 The principal component analysis plot of the fossil data reveals that the eyespot data for
215 individual specimens plot close to the data for the associated host sediment (Figure S9); the
216 data for individual specimens and their sediment do not overlap with those for other fossils.
217 Variation in concentrations of Ca, Fe and Cu among specimens are significantly different

218 (Ca: Welch F: $df = 2.668$, $F = 37.62$, $p = 0.01109$; Fe: ANOVA: $df = 8$, $F = 162$, $p = 6.01^{-06}$;
219 Cu: Welch F: $df = 2.983$, $F = 13.7$, $p = 0.03136$; posthoc tests: Rogers et al. 2020 (Table S4)).
220 Concentrations of Zn do not differ significantly among specimens (Kruskal-Wallis H (χ^2) =
221 0.3556, $p = 0.8371$).

222

223 Differences in concentrations of Cu between the fossil eyespots and the host sediment are
224 significantly different for each fossil specimen (Rogers et al. 2020 (Table S4)). In addition,
225 concentrations of Fe (and, in *Dapalis*, Ca) are significantly different between the eyespot of
226 *Knightia* and the respective host sediment; similarly, concentrations of Fe and Ca differ
227 significantly between the eye of *Dapalis* and the host sediment. Differences in concentrations
228 of Zn between eyespots and host sediment are not significantly different for any of the three
229 fossils analyzed (Rogers et al. 2020 (table S4)).

230

231 LDA plots of the total dataset reveal three major groupings in the LDA chemospace (Fig.
232 3A): (1) fossil melanosomes, (2) melanosome extracts matured in Cu-solution and Cu-Zn-
233 solution, and (3) melanosome extracts matured in DD water, in Zn-solution and untreated
234 melanosomes. The primary elements driving this chemical variation are Ca, Cu and Zn (Fig.
235 3B); in particular, fossil melanosomes have significantly lower concentrations of Zn than
236 untreated modern equivalents (Kruskal-Wallis (H (χ^2) = 12.79, 0.0003). Fossil and
237 untreated modern melanosomes do not differ significantly in concentrations of Ca (Kruskal-
238 Wallis H (χ^2) = 1.421, $p = 0.233$), Cu (H (χ^2) = 0.002, $p = 0.965$) or Fe ($F = (1, 16) =$
239 3.478, $p = 0.081$) (Rogers et al. 2020 (Table S5)). In the total dataset, however, differences in
240 Cu concentrations between samples are significant (Kruskal-Wallis (H (χ^2) = 7.2, 0.02732);
241 differences in concentrations of Ca (Kruskal-Wallis (H (χ^2) = 5.422, 0.06646), Fe (Kruskal-

242 Wallis ($H(\chi^2) = 5.6, 0.06081$) and Zn (Kruskal-Wallis ($H(\chi^2) = 0.3556, 0.8371$)) are not
243 significant.

244

245 Cu-XANES spectra for all samples analyzed have a dominant peak centred at $8\,997.5 \pm 1$ eV
246 showing a major contribution from Cu(II) (Fig. 3C). Only the Cu-XANES profile from the
247 eyespot of *D. macrurus* shows a distinct pre-edge feature at $8\,984.5$ eV, indicating a
248 contribution from Cu(I).

249

250 **DISCUSSION**

251 The results of our study reveal that the metal inventory of eye melanosomes is not
252 significantly altered by maturation in DD water (Fig. 1A–B). This suggests that melanosome-
253 metal associations should persist in natural diagenetic scenarios where pore fluids have low
254 concentrations of metal ions and, since pH decreases with increasing temperature, where pH
255 does not vary markedly. In contrast, melanosome extracts matured in Cu and/or Zn solutions
256 differ in chemistry to untreated samples, and to each other. This confirms that the metal
257 inventory of melanosomes is highly sensitive to local ionic concentrations during diagenesis.

258

259 Metals commonly bind to three functional groups within the eumelanin molecule (OH^- , NH_4^+
260 and COOH^-) (Hong *et al.* 2004); Cu can also be accommodated within the eumelanin
261 porphyrin structure, which may survive diagenesis in at least some fossils (Wogelius *et al.*
262 2011). In *Sepia* melanin, Fe(III) can bind to NH_4^+ or OH^- (Hong *et al.* 2004); Ca(II) and
263 Zn(II) bind to COOH^- and Cu(II) binds primarily to OH^- . In all cases eumelanin-bound
264 metals are strictly co-ordinated to light elements (i.e., O/N). Unlike eumelanin, phaeomelanin

265 comprises monomers (benzothiazine and benzothiazole) that contain S and can chelate Zn
266 (Manning et al. 2019); whether the phaeomelanin S-groups (and other groups present, e.g.
267 NH^-) commonly bind other metals is unclear.

268

269 Extracts matured in Cu-solution are enriched in Cu and depleted in Zn relative to unmatured
270 melanosomes. Experiments at room temperature and pressure indicate that where Cu
271 concentrations exceed 10 mmol, additional Cu(II) can bind to COOH^- sites normally
272 occupied by Ca(II) and Zn(II) (Hong and Simon 2006), displacing the latter two elements.
273 This is consistent with evidence of Cu-binding to melanin COOH^- groups in fossil feathers
274 (Wogelius *et al.* 2011). In our experiments it is possible that the concentration of the Cu-
275 solutions used (16 mmol) was sufficiently high to trigger replacement of Zn(II) by Cu(II) at
276 COOH^- sites during maturation. Experiments on artificial eumelanin, however, show a
277 decrease in COOH^- with thermal maturation (Ito *et al.* 2013). Elevated Cu concentrations in
278 our experiments may therefore reflect (at least in part) the binding of Cu to unoccupied OH^-
279 or NH_4^+ rather than COOH^- .

280

281 Surprisingly, Zn concentrations decrease even when melanosome extracts are matured in
282 solutions containing Zn. Following saturation of COOH^- groups with Zn(II), NH_4^+ and OH^-
283 groups can present secondary binding sites for Zn(II) (Hong and Simon 2006). Melanin,
284 however, has a much higher overall binding affinity for Cu(II) than for Zn(II) (Hong and
285 Simon 2007) and thus Zn(II) may be unable to bind to OH^- groups in melanin when they are
286 already occupied by Cu(II). Low Zn concentrations in melanosomes matured in Cu-Zn-
287 solutions may therefore reflect the following: (1) saturation of OH^- groups by Cu(II) from the
288 experimental medium and the inability of Zn(II) to displace melanin-bound Cu(II) at these

289 sites, and (2) a decrease in the abundance of COOH⁻ bonds due to thermal maturation (Ito *et*
290 *al.* 2013).

291

292 The decrease in Zn concentrations in melanosomes matured in Zn-solutions (i.e., where
293 saturation of OH⁻ groups by Cu(II) cannot occur, as in experiments with Cu-solution) is also
294 consistent with a maturation-induced decrease in available COOH⁻ (Ito *et al.* 2013). This
295 indicates that the original COOH⁻-Zn bond present in the untreated extracts was unstable
296 under the conditions used in our experiments.

297

298 Concentrations of Fe do not differ among untreated and treated melanosomes. This is
299 somewhat surprising because melanin has a higher affinity for Cu(II) than Fe(III) (Hong and
300 Simon, 2007) and thus Cu(II) may be expected to replace Fe(III) at the OH⁻ group (to which
301 Cu commonly binds (Hong and Simon 2007)) and the NH₄⁺ group (to which it binds when
302 present in concentrations <10 mmol (Hong and Simon 2006)). Instead, our data suggest that
303 the additional Cu(II) has not displaced Fe(III) at OH⁻ and NH₄⁺ groups but is bound
304 elsewhere, either to unoccupied functional groups or to COOH⁻ groups in which Cu(II)
305 replaces previously bound metals such as Zn(II).

306

307 Patterns of Ca enrichment and depletion in our dataset are complex. Relative to untreated
308 samples, melanosome extracts are depleted in Ca when matured in Zn and Cu-Zn-solutions
309 but concentrations of Ca are the same when extracts are matured in Cu-solution (Fig. 2). This
310 may reflect changes in pH during the experiments. Metal binding sites in *Sepia* melanin are
311 sensitive to changes in pH; more specifically, increased acidity (e.g. a change from pH 7 to

312 pH 2) results in a decrease in the concentration of elements bound to COOH⁻ groups (Liu *et*
313 *al.* 2004). This reflects protonation of COOH⁻ groups by H⁺ and associated replacement of
314 chelated metals such as Ca(II) (Liu *et al.* 2004). The exact reasons why this occurs in
315 melanosome extracts matured with Zn and Cu-Zn-solutions but not in extracts matured only
316 in Cu solutions is unclear but it may reflect differences in temporal changes in pH evolution
317 in different experimental settings.

318

319 The suspension of melanin in low pH Cu- and/or Zn-solutions in our experiments may have
320 resulted in the replacement of COOH⁻-bound Ca(II) and Zn(II) by H⁺. This process cannot,
321 however, explain the high Ca concentrations in extracts matured in Cu-solution, the origin of
322 which remains unclear. The persistence of Ca(II) in thermally matured samples implies either
323 the survival of some COOH⁻ groups under conditions understood to induce decarboxylation
324 (Ito *et al.* 2013) or binding of Ca(II) to other functional groups in melanin or associated
325 proteins within the melanosome. It is possible that the Ca signal could reflect contributions
326 from other recalcitrant tissue components of the eye, but this is unlikely given that the
327 extracts comprise near-pure agglomerations of melanosomes.

328

329 Our experiments provide an empirical basis for interpreting the chemistry of fossil
330 melanosomes and, in particular, can help us interpret key chemical differences between these
331 and modern melanosomes. Differences in chemistry between the fossil specimens studied
332 may reflect taxonomic or biota-level differences; the small sample size prevents
333 discrimination of these interpretations. Given other evidence for pervasive biota-level control
334 on fossil melanosome chemistry (Rossi *et al.*, 2020), the chemical differences among the
335 specimens in this study likely represent a sedimentary signal (Rogers *et al.* 2020 (Fig. S9)).

336 The consistent offset in the chemical data for eyespots (especially enrichment of Cu) relative
337 to the host sediment could indicate retention of a component of original chemistry (i.e.
338 naturally elevated concentrations of Cu similar to those *in vivo*) or concentration of elements,
339 especially Cu, in fossil melanosomes during diagenesis.

340

341 Direct comparison of the fossil and experimental data reveal that both fossil and thermally
342 matured melanosomes are strongly depleted in Zn relative to unmatured samples. This
343 supports our experimental data on Zn mobility during diagenesis and suggests that the Zn
344 concentrations in the fossils are not original but likely lower than *in vivo*. In natural settings,
345 any Zn(II) displaced as a result of a decrease in pH is likely to be mobilized and lost from the
346 system. Alternatively, displaced Zn may be rendered unavailable for re-chelation by fossil
347 melanin via incorporation into inorganic mineral precipitates in the host sediment.

348

349 A decrease in pH could occur relatively early *postmortem* via the release of organic acids
350 during decay (Briggs and Kear 1993) or through contact with pore waters rich in H⁺ ions.
351 Higher temperatures at deeper burial conditions would also lower pH, further promoting the
352 loss of Zn from fossil melanosomes. Degradation of phaeomelanin (and loss of key Zn
353 binding sites including S²⁻ and OH⁻ (Manning *et al.* 2019)) during diagenesis could lead to a
354 further depletion of Zn. This process is unlikely to contribute significantly to our
355 experimental data, however, as the eye melanin of *D. labrax* is dominated by eumelanin *in*
356 *vivo* (Rogers *et al.* 2019) and most or all phaeomelanin originally present in the tissue is
357 likely to have been degraded during enzymatic extraction (Liu *et al.* 2005). Uplift and
358 exposure would presumably result in an increase in local pH, but it is unclear whether
359 thermally altered melanin could bind available Zn in this scenario, especially given that

360 thermal maturation is associated with decarboxylation of melanin (Ito *et al.* 2013) and thus
361 loss of preferred functional groups for Zn-melanin chelation.

362

363 Ca, Fe and Cu concentrations are similar in fossil melanosomes and unmaturred extracts. This
364 suggests that original associations between Ca(II), Fe(III) and Cu(II) and melanin may have
365 been retained. Melanin, however, has a lower binding affinity for Ca(II) than Zn(II) (Hong
366 and Simon 2007); given that Zn was lost from matured melanosomes in our experiments it
367 thus seems unlikely that original associations between Ca(II) and melanin would survive
368 diagenesis. Instead, it is plausible that Ca concentrations in the matured melanosome extracts
369 may reflect loss early during diagenesis and subsequent re-binding of Ca(II) once local pH
370 and ionic conditions become more favourable. This suggests that the melanin molecule may
371 retain a dynamic relationship with its environment long into diagenesis. Other metals such as
372 Fe and Cu, originally bound to melanin, could also be lost and rebound in this fashion.
373 Alternatively, some Ca, Fe and Cu associated with fossil eye melanosomes may have been
374 bound to non-melanin labile organic components *in vivo*. Breakdown of those compounds
375 during diagenesis and subsequent incorporation of metal ions into remnants of the melanin
376 molecule (Wogelius *et al.* 2011) could contribute to concentrations of these metals in fossil
377 melanosomes, but this hypothesis requires testing. Although biomolecules are understood to
378 undergo the loss of functional groups during diagenesis (Eglington *et al.* 1991, Ito *et al.* 2013),
379 our results suggest at least some of these functional groups must survive this process and
380 remain viable binding sites for various metal ions.

381

382 Application of these SRS-XRF data to fossils strongly suggests that low Zn concentrations
383 and low Zn: Cu ratios in some fossil vertebrate eye melanosomes are a diagenetic artefact

384 (Fig. 4). Our previous study revealed that eye melanosomes in fossil vertebrates have low Zn
385 relative to extant analogues (Rogers et al. 2019). Our experimental data reveal that this likely
386 reflects the loss of Zn and/or the replacement of Zn by Cu during diagenesis. Variation in the
387 chemistry of melanosomes preserved in fossils from different biotas likely reflects different
388 ionic concentrations, pH and burial regimes during diagenesis (Rogers *et al.* 2019). Variation
389 in diagenetic regime, however, is less likely to explain spatial heterogeneity in melanin
390 chemistry within a single fossil. In the latter scenario chemical variation is more likely to
391 reflect biological factors, e.g. original variation in eu- and phaeomelanin content due to
392 integumentary patterning (Wogelius et al. 2011) and/or enrichment in various internal organs
393 (Rossi et al. 2019, 2020). Higher concentrations in some fossil vertebrates, especially those
394 hosted within concretions (such as those from the Mazon Creek), may reflect rapid
395 cementation of the host sediment, limiting interactions of pore fluids with melanosomes (and
396 thus loss of Cu and Zn) later during diagenesis.

397

398 Cu-XANES spectra for matured and untreated melanosomes are dominated by signals for
399 Cu(II). The local binding environment of melanosomal Cu clearly does not alter substantially
400 during maturation (Fig. 3C). The presence of a Cu(I) signal in fossil melanosomes from
401 *Dapalis* could reflect an artefact of the XANES analysis whereby some Cu(II) was reduced
402 during analysis. Other vertebrate fossils (Wogelius *et al.* 2011; Rogers *et al.* 2019) and
403 modern melanosomes analyzed under identical conditions, however, do not show a
404 contribution from Cu(I). Instead, the Cu(I) contribution to the *Dapalis* XANES spectrum may
405 be a real signal, reflecting local conditions during diagenesis.

406

407 In conclusion, our study reveals the effects of diagenesis on trace element chemistry of
408 melanosomes. Specifically, our data confirm that relatively low concentrations of Zn in fossil
409 vertebrate eye melanosomes is likely to be a diagenetic feature and that this depletion in Zn
410 relative to modern eye melanosomes is controlled, in large part, by local ionic and pH
411 conditions during diagenesis and not by elevated temperatures and pressures alone. Our
412 experiments also show that original concentrations of Ca and Cu in melanosomes are
413 susceptible to changes during maturation. The fossils we studied show considerable variation
414 in the concentrations of Ca and Cu, likely due to variations in the diagenetic history of the
415 deposit. Our data also reveal that the oxidation state of Cu is not altered under conditions of
416 our maturation experiments, but that it may be altered during fossilization. These results
417 confirm that components of the preserved trace element chemistry of fossil melanosomes
418 could be a diagenetic artefact and that maturation experiments can yield essential insights
419 into the chemical taphonomy of melanosomes that should be incorporated into future
420 interpretations of preserved chemical signatures in fossils.

421

422 Collectively, our data emphasise the dynamic nature of links between fossil chemistry and the
423 host sediment, in particular variations in pore fluid chemistry, through time. Melanin
424 elemental chemistry is clearly plastic during diagenesis. Other, more labile, components of
425 fossil chemistry, e.g. proteins (Asara et al. 2007, Schweitzer et al. 2007, Schweitzer et al.
426 2013, Schroeter et al. 2017) and nucleic acids (Schweitzer et al. 2013, Bailleul et al. 2020),
427 would presumably be equally, if not more, susceptible to alteration during decay and
428 diagenesis.

429

430 *Acknowledgements.* We thank Nick Edwards and Sharon Bone for XAS and XRF support, T.
431 Clements, T. Slater, V. Rossi for help with XAS and XRF data acquisition and helpful
432 discussion. Supported by European Research Starting Grant (grant no. ERC-2014-StG-
433 637691-ANICOLEVO) awarded to M.E.M. The use of the Stanford Synchrotron Radiation
434 Lightsource, SLAC National Accelerator Laboratory, is supported by the US Department of
435 Energy, Office of Science, Office of Basic Energy Sciences under contract no. DE-AC02-
436 76SF00515 via beamtime proposals 4615 and 5072 awarded to M.E.M.

437 *Author contributions.* M.E.M. and C.S.R. conceived the study; C.S.R., M.E.M. and S.M.W.
438 performed synchrotron rapid scanning-X-ray fluorescence and X-ray absorption spectroscopy
439 (XAS); C.S.R. and M.E.M. wrote the manuscript with input from S.M.W.

440 *Supplementary data.* All data is provided in the main text or via the Dryad Digital
441 Repository:
442 <https://datadryad.org/stash/share/H5aMNvcCsDvpSa94b2Wf8T69ZSdwLc3Cb9zMAI0hn4>.

443 **References:**

- 444 AGIUS, C. and ROBERTS, R. J. 2003. Melano-macrophage centres and their role in fish
445 pathology. *Journal of Fish Diseases*, **26**, 499–509.
- 446 ASARA, J. M., SCHWEITZER, M. H., FREIMARK, L. M., PHILLIPS, M. and CANTLEY,
447 C. L. 2007. Protein sequences from mastodon and *Tyrannosaurus rex* revealed by mass
448 spectrometry. *Science*, **316**, 280–285.
- 449 BAILLEUL, A. M., ZHENG, W., HORNER, J. R., HALL, B. K., HOLLIDAY, C. M. and
450 SCHWEITZER, M. H. 2020. Evidence of proteins, chromosomes and chemical markers of
451 DNA in exceptionally preserved dinosaur cartilage. *National Science Review*, **7**, 815–822.

452 BRENNER, M. and HEARING, V. J. 2007. The protective role of melanin against UV
453 damage in human skin. *Photochemistry and Photobiology*, **84**, 539–549.

454 BRIGGS, D. E. G. and KEAR, A. J. 1993. Fossilization of soft tissue in the laboratory.
455 *Science*, **259**, 1439–1442.

456 CHEN, S., XUE, C., WANG, J., FENG, H., WANG, Y., MA, Q. and WANG, D. 2009.
457 Adsorption of Pb(II) and Cd(II) by squid *Ommastrephes bartrami* melanin. *Bioinorganic*
458 *Chemistry and Applications*, **2009**, 901563.

459 COLLEARY, C., DOLOCAN, A., GARDNER, J., SINGH, S., WUTTKE, M.,
460 RABENSTEIN, R., HABERSETZER, J., SCHAAL, S., FESEHA, M., CLEMENS, M.
461 and JACOBS, B. F., CURRANO, E. D., JACOBS, L. L., LYNG SYLVESTERSEN, R.,
462 GABBOTT, S. E. and VINTHER, J. 2015. Chemical, experimental and morphological
463 evidence for diagenetically altered melanin in exceptionally preserved fossils. *Proceedings*
464 *of the National Academy of Sciences USA*, **112**, 12592–12597.

465 EGLINGTON, G. and LOGAN, G. A. 1991. Molecular preservation. *Philosophical*
466 *Transactions of the Royal Society of London. Series B: Biological Sciences*, **333**, 315–328.

467 GAUDANT, J. 2015. Présence du genre *Lepidocottus* Sauvage, 1875 (Teleostei, Gobioidi)
468 dans l'Oligocène inférieur des environs de Céreste (Alpes-de-Haute-Provence, France).
469 *Geodiversitas*, **37**, 229–235.

470 HAMMER, Ø., HARPER, D. A. T. and RYAN, P. D. 2001. PAST: Paleontological statistics
471 software package for education and data analysis. *Palaeontologica Electronica*, **4**, 9.

472 HONG, L. and SIMON, J. D. 2006. Insight into the binding of divalent cations to *Sepia*
473 eumelanin from IR absorption spectroscopy. *Photochemistry and Photobiology*, **82**, 1265–
474 1269.

475 ———— 2007. Current understanding of the binding site, capacity, affinity, and
476 biological significance of metals in melanin. *Journal of Physical Chemistry B*, **111**, 7938–
477 7947.

478 HONG, L., LIU, Y. and SIMON, J. D. 2004. Binding of metal ions to melanin and their
479 effects on the aerobic reactivity. *Photochemistry and Photobiology*, **80**, 477–481.

480 ITO, S., WAKAMATSU, K., GLASS, K., SIMON, J.D. 2013. High-performance liquid
481 chromatography estimation of cross-linking of dihydroxyindole moiety in eumelanin.
482 *Analytical Biochemistry*, **434**, 221–225.

483 LINDGREN, J., UVDAL, P., SJÖVDALL, P., NILSSON, D. E., ENGDAHL, A.,
484 SCHULTZ, B. P. and THIEL, V. 2012. Molecular preservation of the pigment melanin in
485 fossil melanosomes. *Nature Communications*, **3**, 824.

486 LIU, Y., HONG, L., WAKAMATSU, K., ITO, S., ADHYARU, B., CHENG, C. Y.,
487 BOWERS, C. R., and SIMON, J. D. 2005. Comparison of structural and chemical
488 properties of black and red human hair melanosomes. *Photochemistry and Photobiology*,
489 **18**, 135–144.

490 LIU, Y., HONG, L., KEMPF, V. R., WAKAMATSU, K., ITO, S. and SIMON, J. D. 2004.
491 Ion-exchange and adsorption of Fe(III) by *Sepia* melanin. *Pigment Cell Research*, **17**,
492 262–269.

493 LOEWEN, M. A., and BUCHHEIM, H. P. 1998. Paleontology and paleoecology of the
494 culminating phase of Eocene fossil lake, Fossil Butte National Monument, Wyoming.
495 *National Park Service Paleontological Research Volume 3*, 73-80.

496 MANNING, P. L., EDWARDS, N. P., BERGMAN, U., ANNE, J., SELLERS, W. I., VAN
497 VEELLEN, A., SOKARAS, D., EGERTON, V. M., ALONSO-MORI, R., IGNATYEV, K.,

498 VAN DONGEN, B. E., WAKAMATSU, K., ITO, S., KNOLL, F., and WOGELIUS, R.
499 A. 2019. Pheomelanin pigment remnants mapped in fossils of an extinct mammal. *Nature*
500 *Communications*, **10**, 2250.

501 MCNAMARA, M. E., BRIGGS, D. E. G., ORR, P. J., FIELD, D. J. and WANG, Z. 2013.
502 Experimental maturation of feathers: implications for reconstructions of fossil feather
503 colour. *Biology Letters*, **9**, 20130184.

504 ——— VAN DONGEN, B. E., LOCKYEAR, N. P., BULL, I. D. and ORR, P. J. 2016.
505 Fossilization of melanosomes via sulfurization. *Palaeontology*, **59**, 337–350.

506 NAPPI, A. J. and CHRISTENSEN, B. M. 2005. Melanogenesis and associated cytotoxic
507 reactions: Applications to insect innate immunity. *Insect Biochemistry and Molecular*
508 *Biology*, **35**, 443–459.

509 OAKLEY, T. H. and SPEISER, D. I. 2015. How complexity originates: the evolution of
510 animal eyes. *Annual Review of Ecology, Evolution and Systematics*, **46**, 237–260.

511 PEDERSEN, G. K. and BUCHARDT, B. 1996. The calcareous concretions (cementsten) in
512 the Fur Formation (Paleogene, Denmark): isotopic evidence of early diagenetic growth.
513 *Bulletin of the Geological Society of Denmark*, **43**, 78–86.

514 RAVEL, B. and NEWVILLE, M. 2005. Athena, Artemis, Hephaestus: data analysis for X-
515 ray absorption spectroscopy using IFEFFIT. *Journal of Synchrotron Radiation*, **12**, 537–
516 541.

517 ROGERS, C. S., ASTROP, T. I., MCNAMARA, M. E., WEBB, S. M., ITO, S. and
518 WAKAMATSU, K. 2019. Synchrotron-X-ray absorption spectroscopy of melanosomes in
519 vertebrates and cephalopods: implications for the affinity of *Tullimonstrum*. *Proceedings*
520 *of the Royal Society B*, **286**, 20191649.

521 ———, WEBB, S. M. and MCNAMARA, M. E. 2020. Data from: Synchrotron-X-ray
522 fluorescence analysis reveals diagenetic alteration of fossil melanosome trace metal
523 chemistry. *Dryad Digital Repository*. <https://datadryad.org/stash/share/XXXX>

524 ROSSI, V., MCNAMARA, M. E., WEBB, S. M., ITO, S. and WAKAMATSU, K. 2019.
525 Tissue-specific geometry and chemistry of modern and fossilized melanosomes reveal
526 internal anatomy of extinct vertebrates. *Proceedings of the National Academy of Sciences*
527 *USA*, **116**, 17880–17889.

528 ———, WEBB, S.M. and MCNAMARA, M.E. 2020. Hierarchical biota-level and
529 taxonomic controls on the chemistry of fossil melanosomes revealed using synchrotron X-
530 ray fluorescence. *Scientific Reports*, **10**, 8970.

531 SCHROETER, E. R., DeHART, C. J. CLELAND, T.P., ZHENG, W., THOMAS, P. M.,
532 KELLEHER, N. L., BERN, M. and SCHWEITZER, M. H. 2017. Expansion for the
533 *Brachylophosaurus canadensis* collagen I sequence and additional evidence of the
534 preservation of Cretaceous protein. *Journal of Proteome Research*, **16**, 920–932.

535 SCHWEITZER, M. H., SUO, Z., RECEP, A., ASARA, J. M., ALLEN, M. A., ARCE, F. T.,
536 and HORNER, J. R. 2007. Analysis of soft tissue from *Tyrannosaurus rex* suggests the
537 presence of protein. *Science*, **316**, 277–280.

538 ———, ZHENG, W., CLELAND, T.P. and BERN, M. 2013. Molecular analyses of dinosaur
539 osteocytes support the presence of endogenous molecules. *Bone*, **52**, 414–423.

540 STANKIEWICZ, A. R., BRIGGS, D. E. G., MICHELS, R., COLLINSON, M. E.,
541 FLANNERY, M. B. and EVERSLED, R. P. 2000. Alternative origin of aliphatic polymer
542 in kerogen. *Geology*, **28**, 559–562.

543 WEBB, S. M. 2011. The microanalysis toolkit: X-ray fluorescence image processing
544 software. *AIP Conference Proceedings*, **1365**, 196–199.

545 WOGELIUS, R. A., MANNING, P. L., BARDEN, H. E., EDWARDS, N. P., WEBB, S. M.,
546 SELLERS, W. I., TAYLOR, K. G., LARSON, P. L., DODSON, P., YOU, H., DA-QING,
547 L. and BERGMANN, U. 2011. Trace metals as biomarkers for eumelanin pigment in the
548 fossil record. *Science*, **333**, 1622–1626.

549

550 **Figure captions:**

551 **Figure 1.** Effect of temperature and pressure on the trace element chemistry of eye
552 melanosomes of *Dicentrarchus* (Actinopterygii: Perciformes). A, Linear Discriminant
553 Analysis chemospace plot based on measured concentrations of Ca, Fe, Cu and Zn in
554 untreated and experimentally matured melanosomes. B, Biplot showing the contribution of
555 each element to variation in A.

556 **Figure 2.** Differences in the concentrations of key elements Ca, Fe, Cu and Zn in
557 melanosome extracts from eyes of *Dicentrarchus*. X-axis labels refer to untreated extracts
558 (UNMAT) and extracts matured under various conditions as follows: Cu T only, Cu-solution
559 with elevated temperature; Cu T&P, Cu-solution with elevated temperature and pressure; Cu
560 & Zn, Cu-Zn-solution with elevated temperature and pressure; DD T only, distilled water
561 with elevated temperature; DD T&P, distilled water with elevated temperature and pressure;
562 Zn, Zn-solution with elevated temperature and pressure; UNMAT, untreated melanosomes.
563 Concentration units are $\mu\text{g}/\text{cm}^2$.

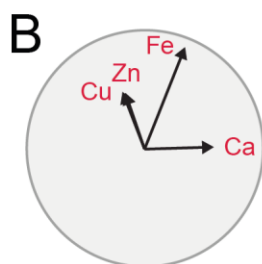
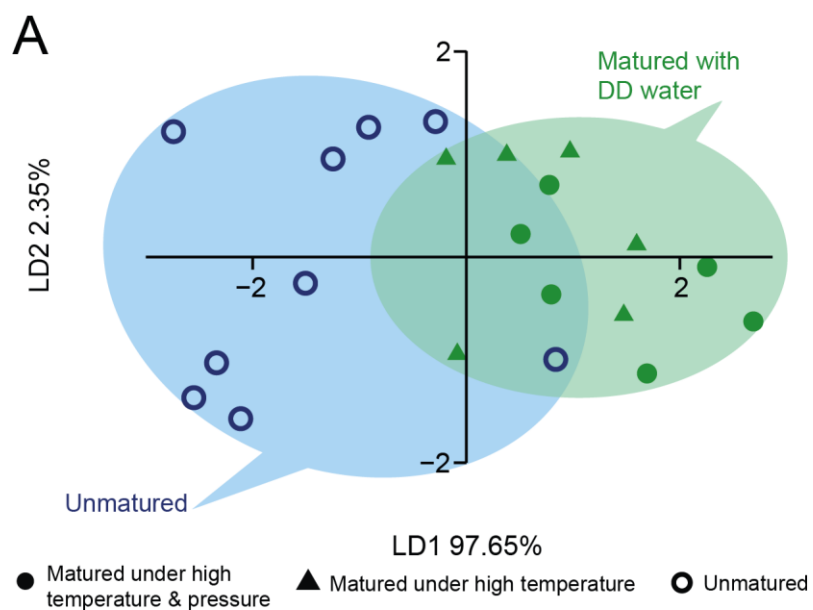
564 **Figure 3.** Comparison of the trace element chemistry of melanosome extracts and fossil
565 melanosomes. A, Linear Discriminant Analysis chemospace plot including data for Ca, Fe,

566 Cu and Zn in unmaturred and matured melanin extracts from eye melanosomes of
567 *Dicentrarchus* and from fossil Teleostei (*Dapalis*, *Knighthia* and Tetradontiformes). B, Biplot
568 of key elements and their contribution to variation in A. C, XANES spectra at the Cu K edge
569 at 8987 eV (dashed line).

570 **Figure 4.** A, Comparison of data on Zn and B, log Zn and Cu chemistry concentrations and
571 log Zn:Cu ratios among matured and unmaturred melanosome extracts and fossil eyespot
572 melanins. X-axis labels refer to fossil specimens, untreated extracts (UNMAT) and extracts
573 matured under various conditions as follows Cu T only, Cu-solution with elevated
574 temperature; Cu T&P, Cu-solution with elevated temperature and pressure; Cu & Zn, Cu-Zn-
575 solution with elevated temperature and pressure; DD T only, distilled water with elevated
576 temperature; DD T&P, distilled water with elevated temperature and pressure; Zn, Zn-
577 solution with elevated temperature and pressure; UNMAT, untreated melanosomes. Data
578 from Mazon Creek (MC) vertebrates, Tetradontiformes and *Knighthia* are from Rogers *et al.*
579 2019. Concentration units are $\mu\text{g}/\text{cm}^2$.

580

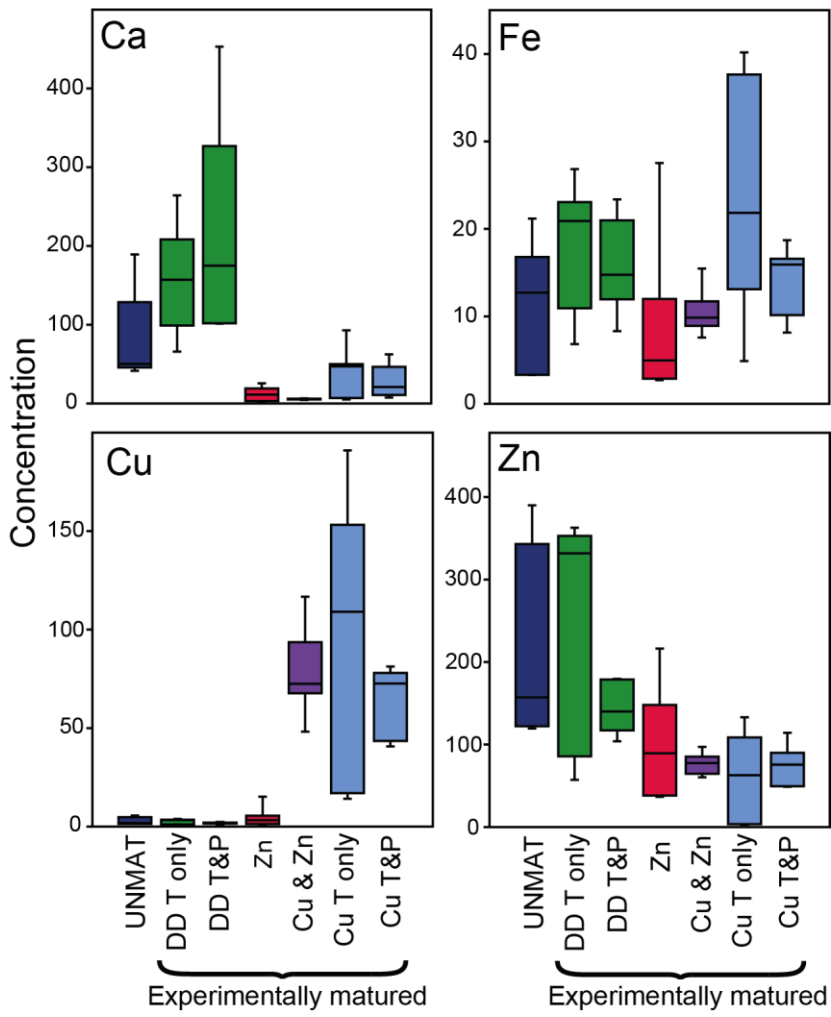
581 **Figure 1.**



582

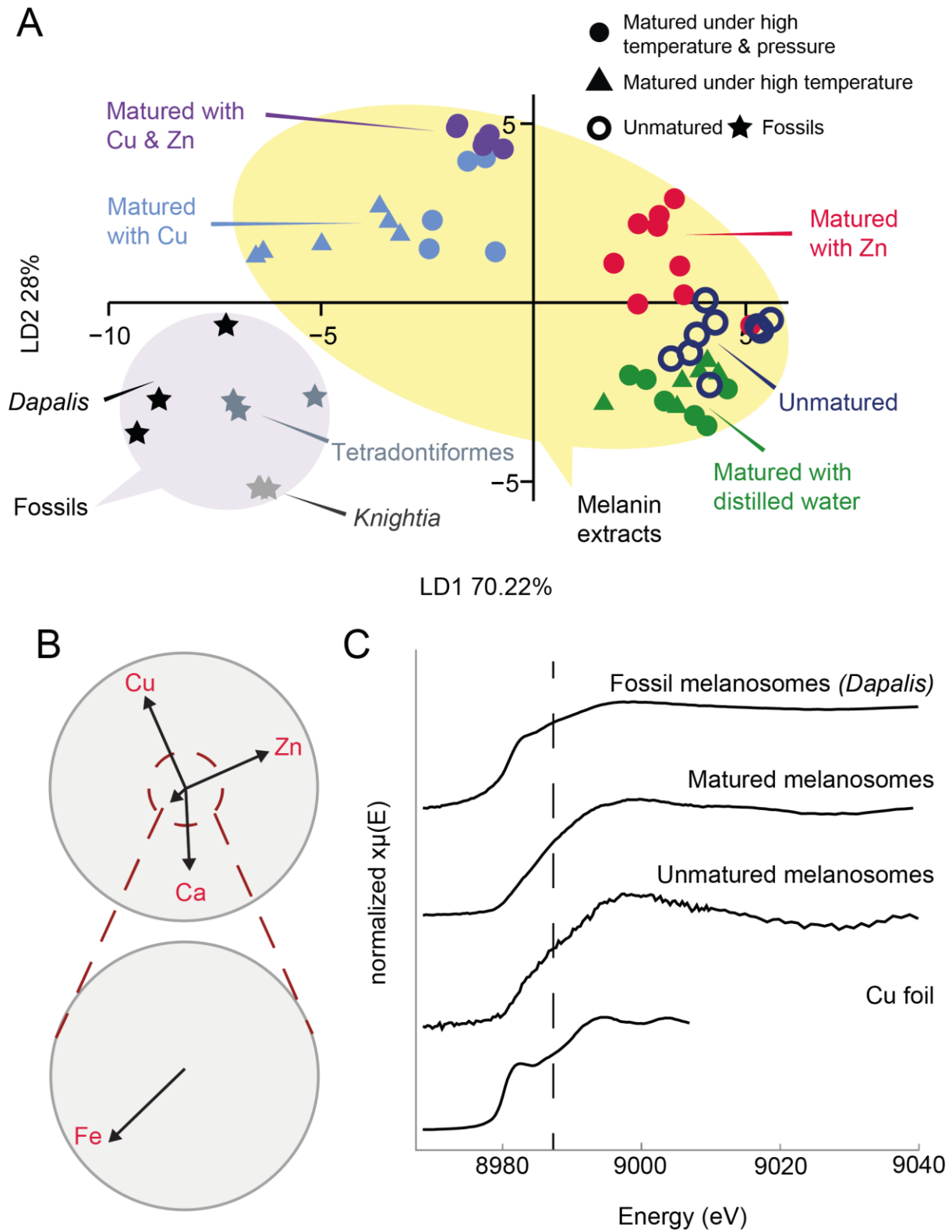
583

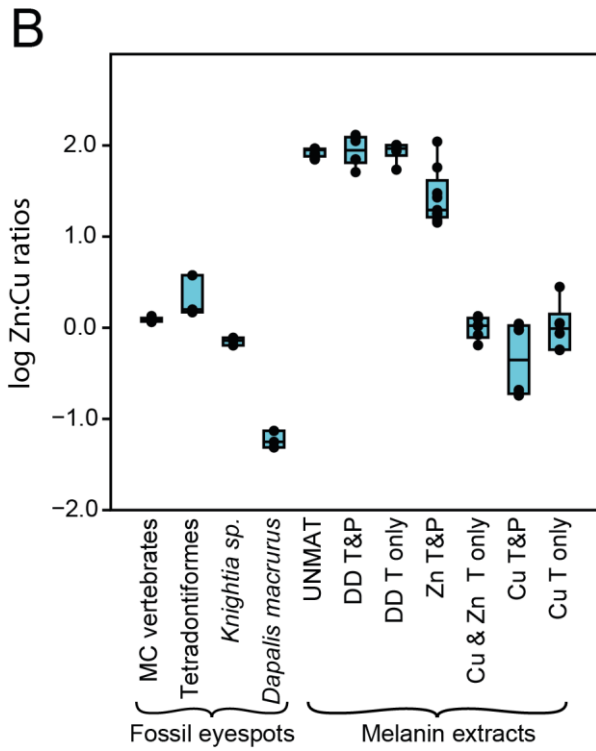
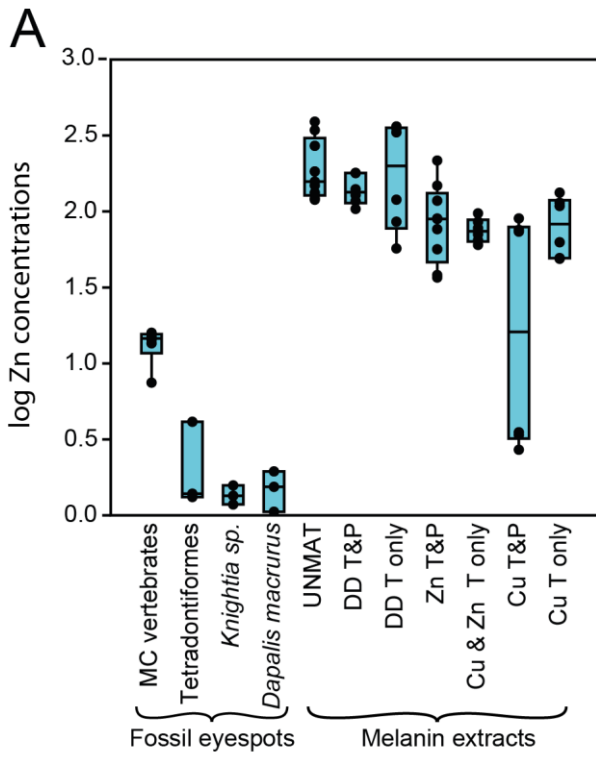
584 **Figure 2.**



585

586





1 **Supplementary Information for**

2

3 **Synchrotron-X-ray fluorescence analysis reveals diagenetic alteration of fossil**
4 **melanosome trace metal chemistry**

5 Christopher S. Rogers, Maria E. McNamara, Samuel M. Webb

6 Christopher S. Rogers, Maria E. McNamara

7 Email: christopher.rogers@ucc.ie; maria.mcnamara@ucc.ie

8

9

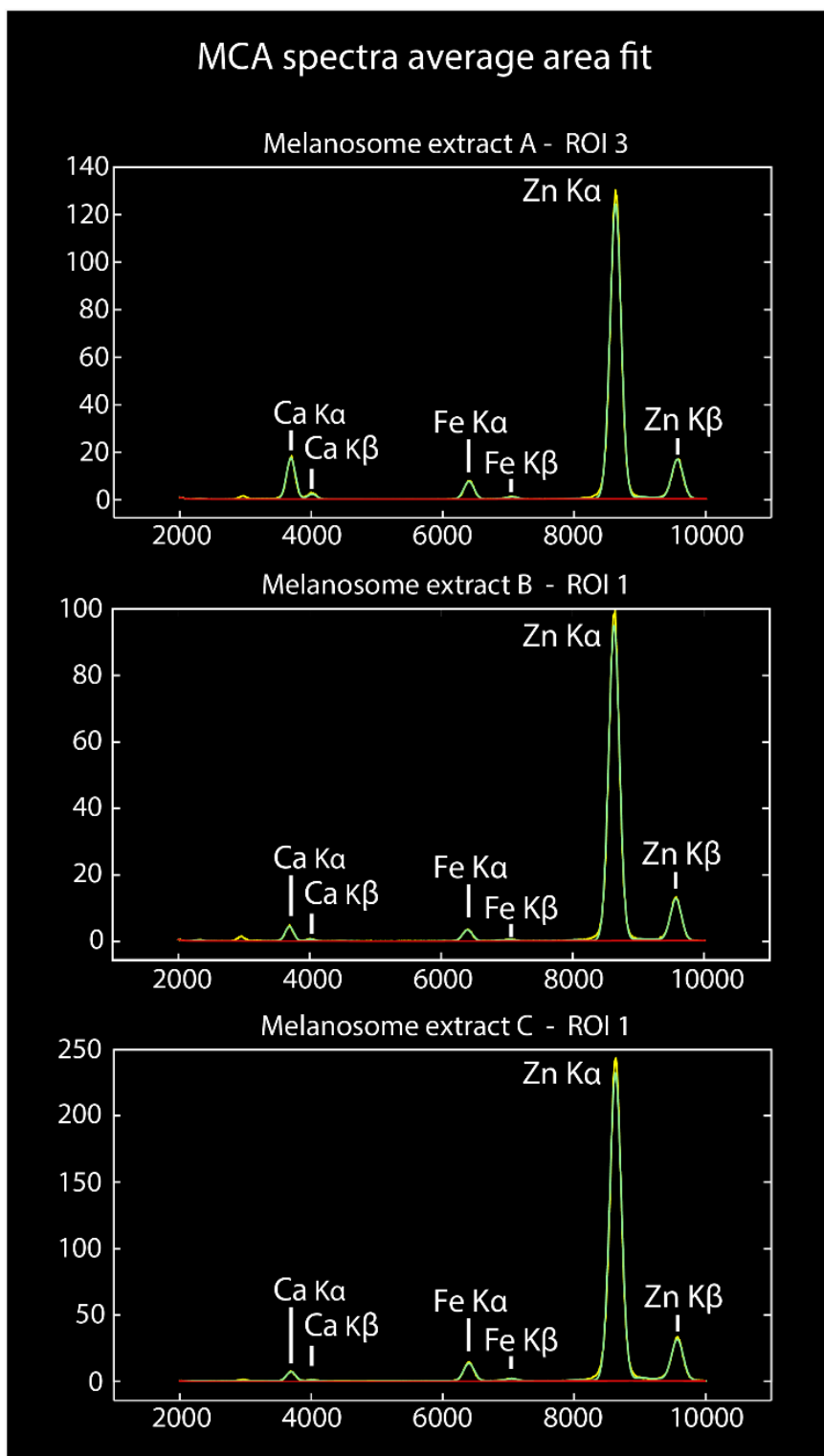
10 **This PDF file includes:**

11

12 Figures S1 to S9

13 Tables S1 to S5

14



15

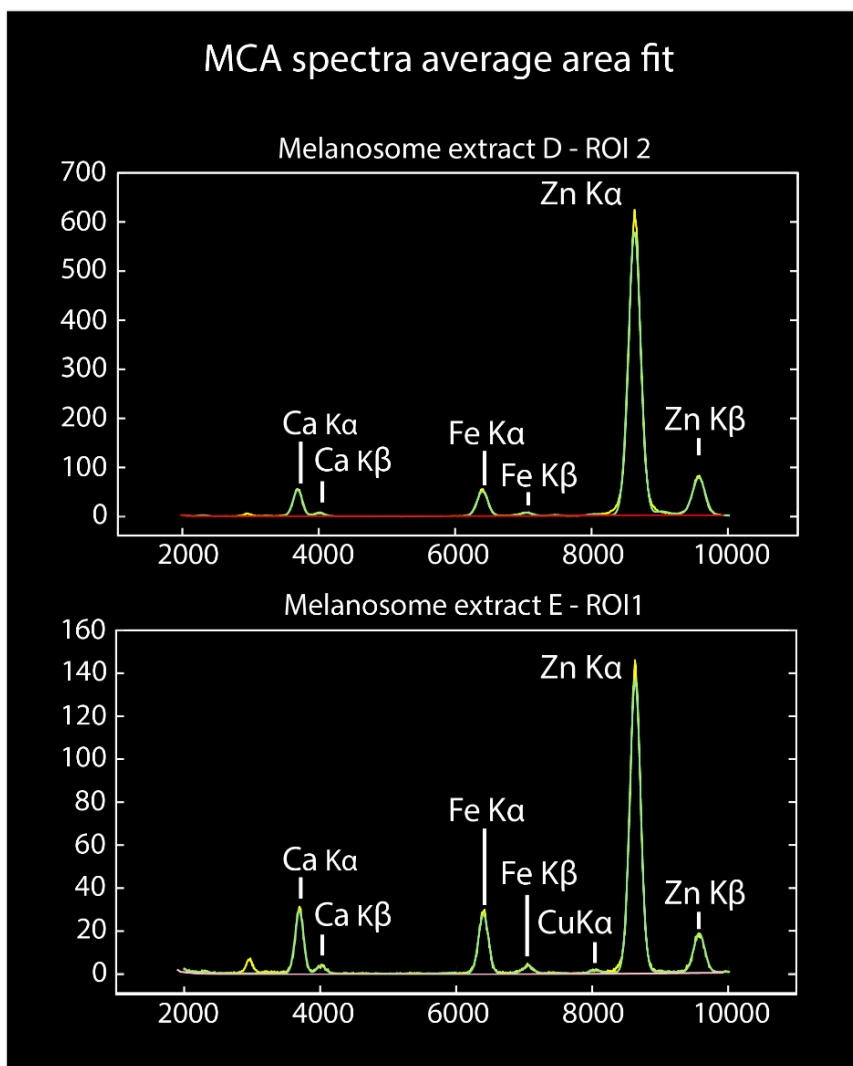
16

17 **Fig. S1.** MCA spectra from regions of interest in SRS-XRF maps of unmaturred melanin extracts A–C.

18 X-axis, X-ray emission energy (keV). Y-axis, counts. Yellow line denotes measured data; green line

19 denotes the computed fit.

20



21

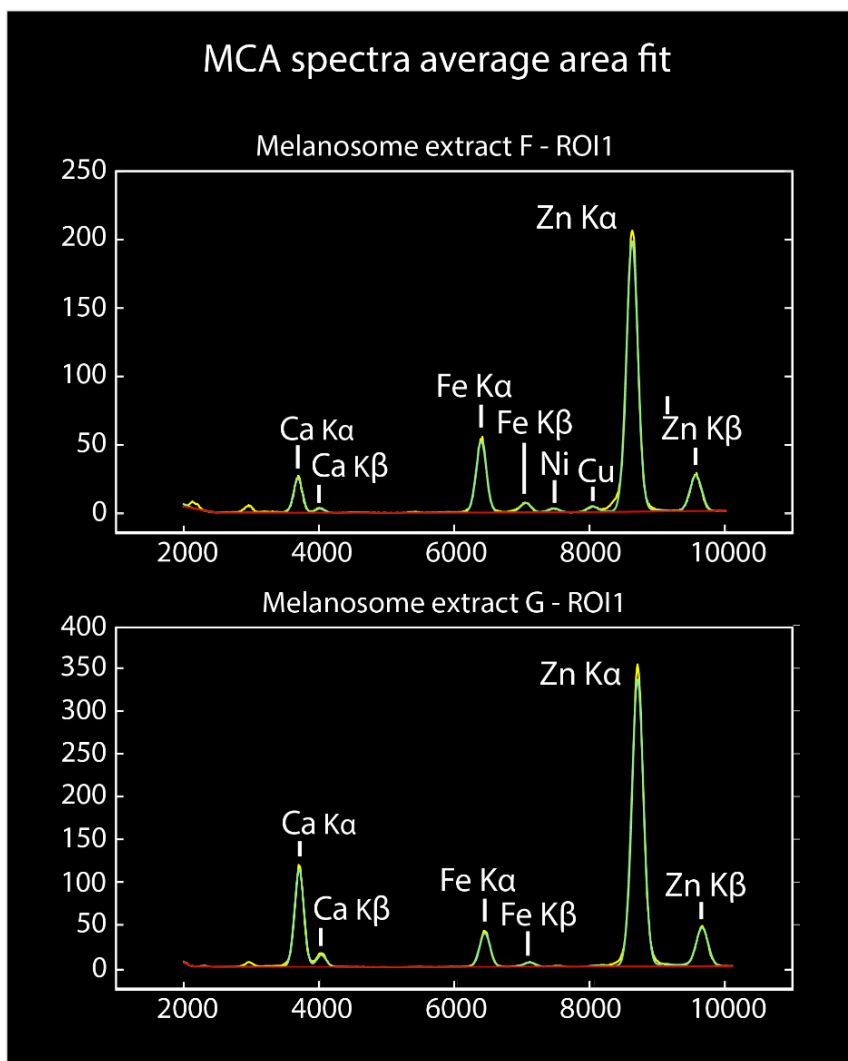
22

23 **Fig. S2.** MCA spectra from regions of interest in SRS-XRF maps of unmaturred melanin extracts D, E.

24 X-axis, X-ray emission energy (keV). Y-axis, counts. Yellow line denotes measured data; green line

25 denotes the computed fit.

26



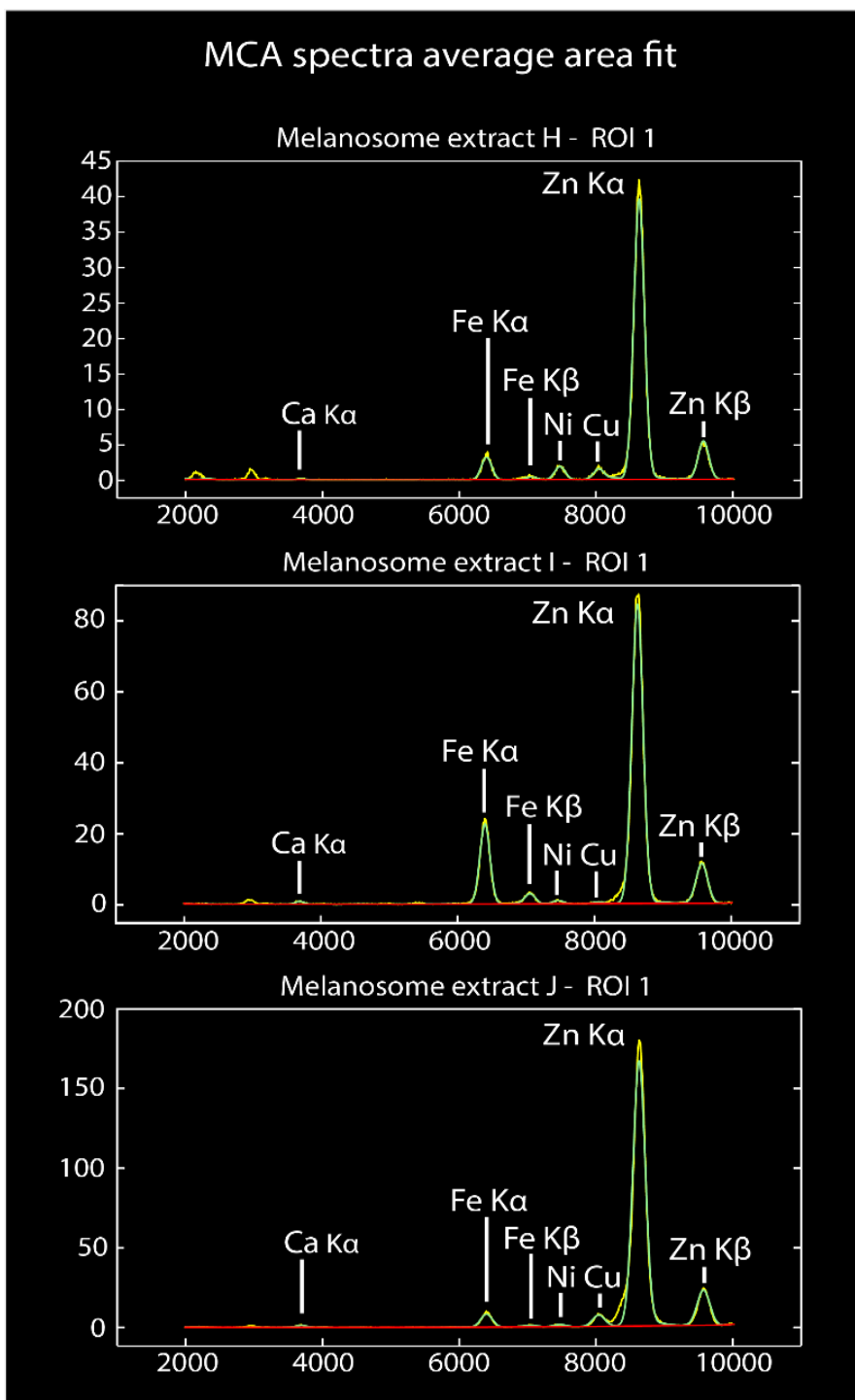
27

28

29 **Fig. S3.** MCA spectra from regions of interest in SRS-XRF maps of unmatured melanin extracts F, G.

30 X-axis, X-ray emission energy (keV). Y-axis, counts. Yellow line denotes measured data; green line

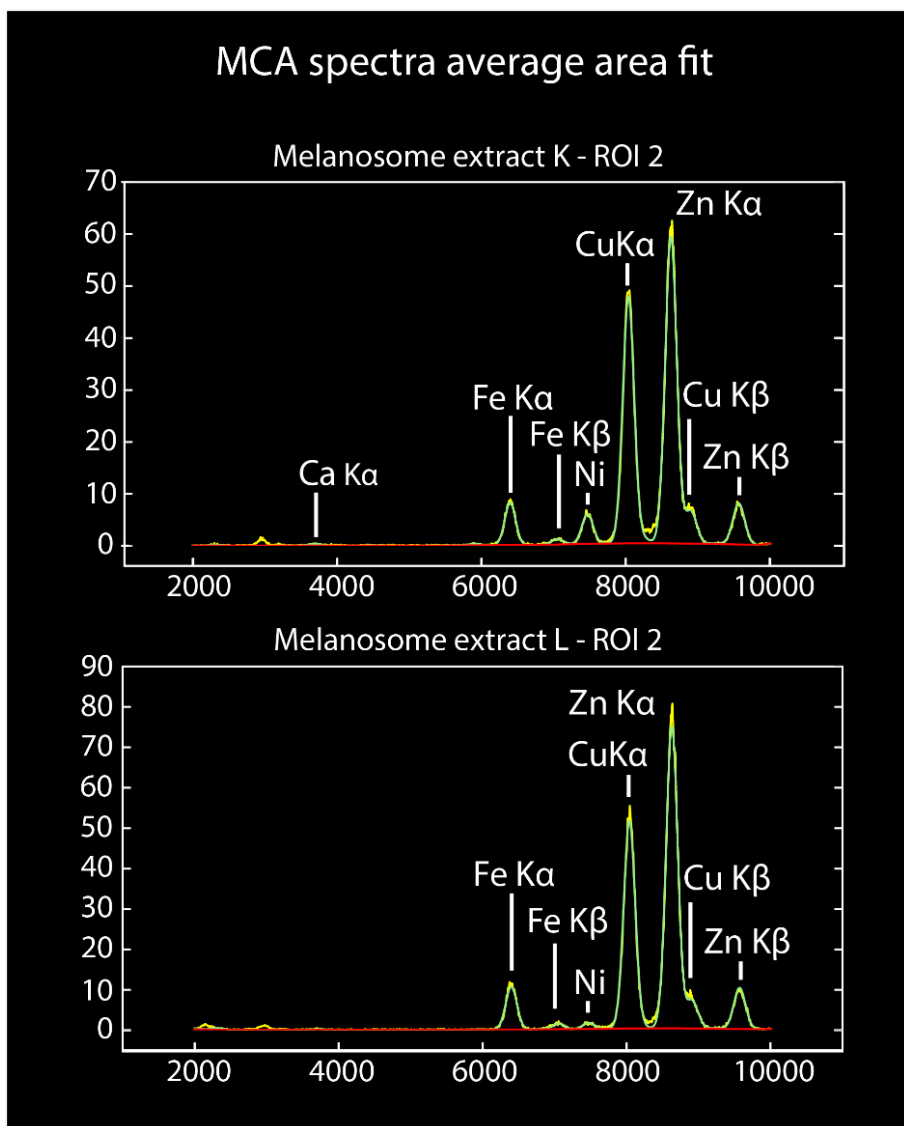
31 denotes the computed fit.



56

57 **Figure S4.** MCA spectra from regions of interest in SRS-XRF maps of unmaturred melanin extracts H,
 58 I, J. X-axis, X-ray emission energy (keV). Y-axis, counts. Yellow line denotes measured data; green
 59 line denotes the computed fit.

60



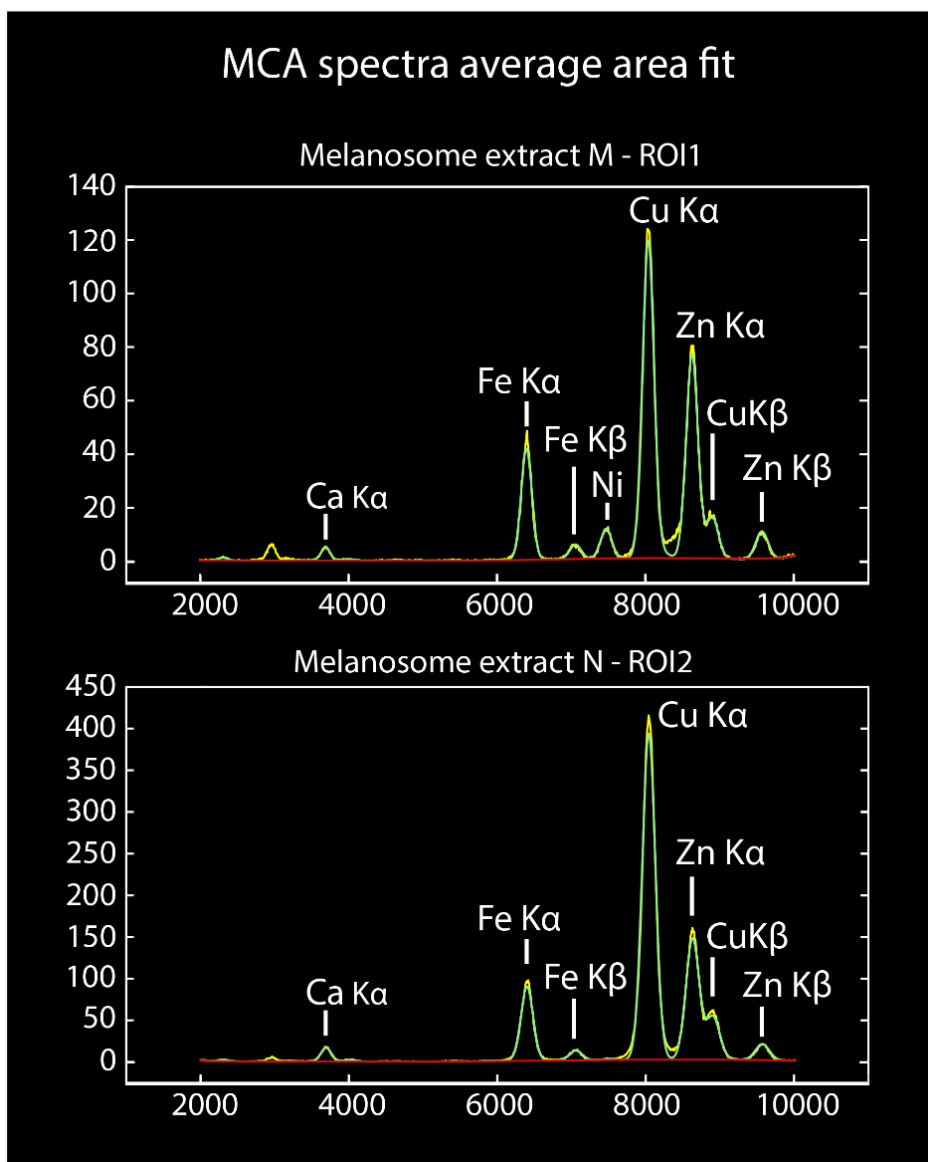
61

62

63 **Fig. S5.** MCA spectra from regions of interest in SRS-XRF maps of unmaturred melanin extracts K, L.

64 X-axis, X-ray emission energy (keV). Y-axis, counts. Yellow line denotes measured data; green line

65 denotes the computed fit.



66

67

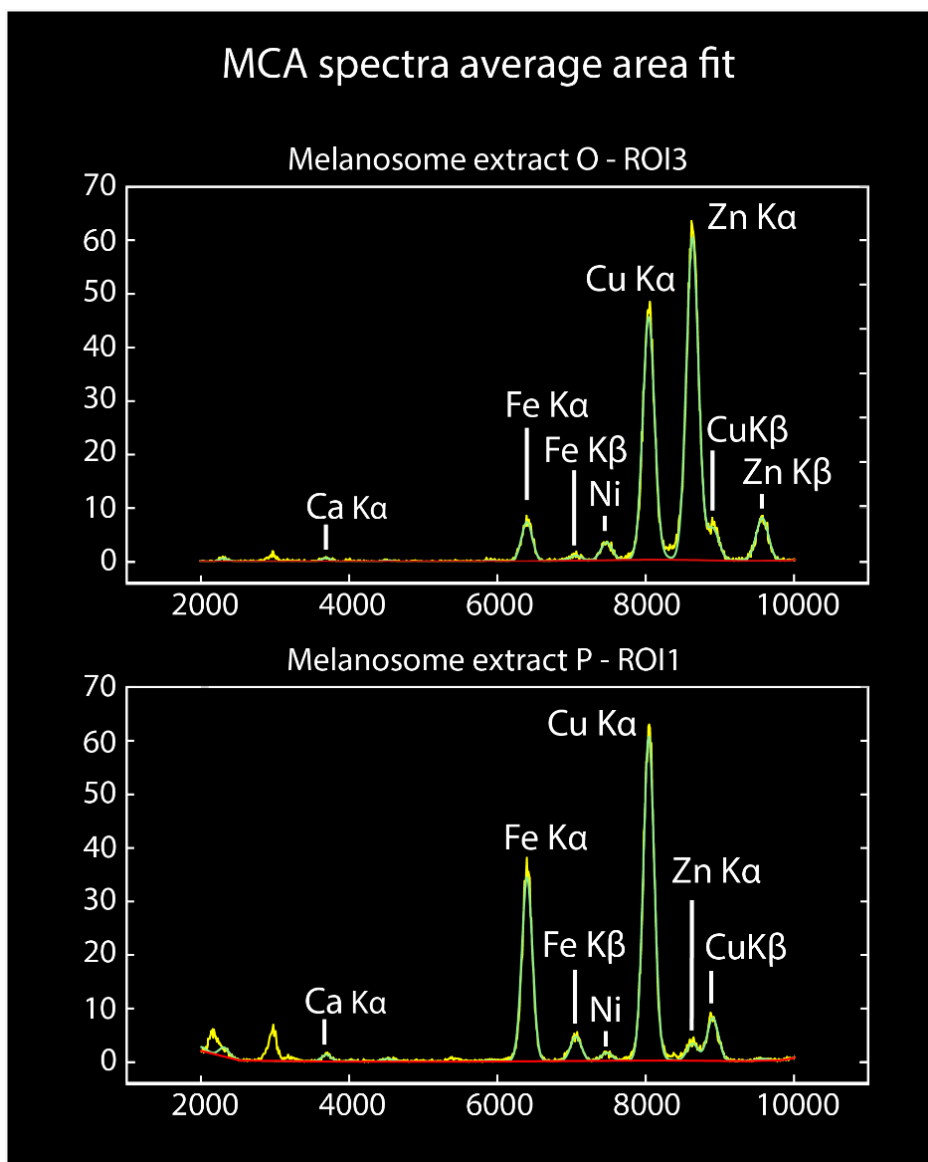
68 **Fig. S6.** MCA spectra from regions of interest in SRS-XRF maps of unmaturred melanin extracts M,

69 N. X-axis, X-ray emission energy (keV). Y-axis, counts. Yellow line denotes measured data; green

70 line denotes the computed fit.

71

72



73

74

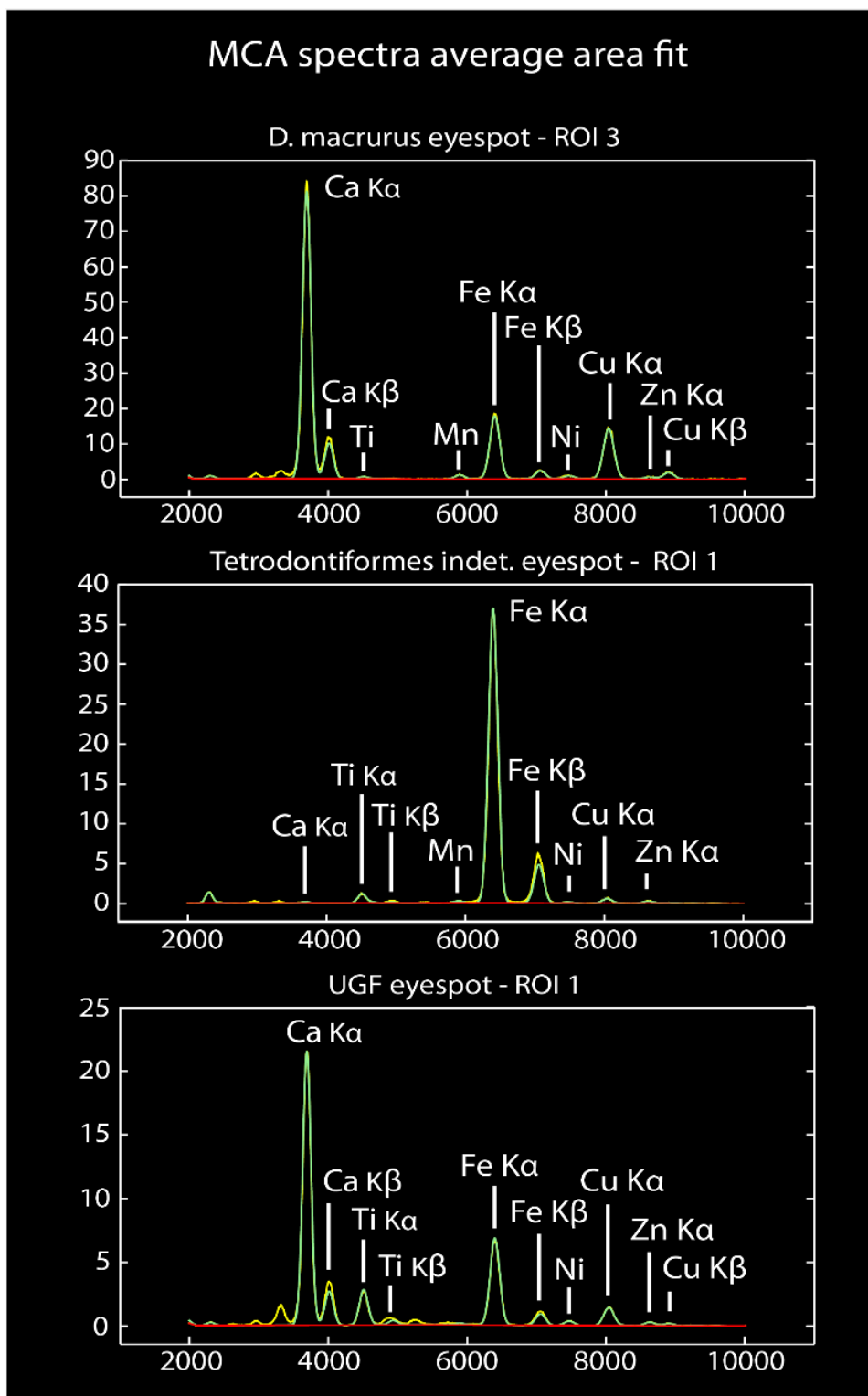
75 **Fig. S7.** MCA spectra from regions of interest in SRS-XRF maps of unmatred melanin extracts O, P.

76 X-axis, X-ray emission energy (keV). Y-axis, counts. Yellow line denotes measured data; green line

77 denotes the computed fit.

78

79



80

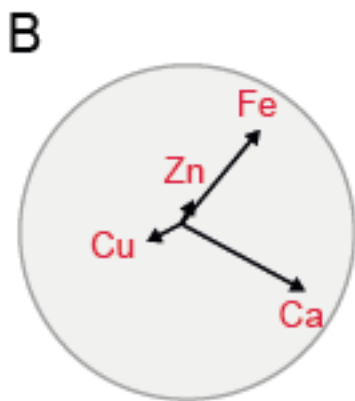
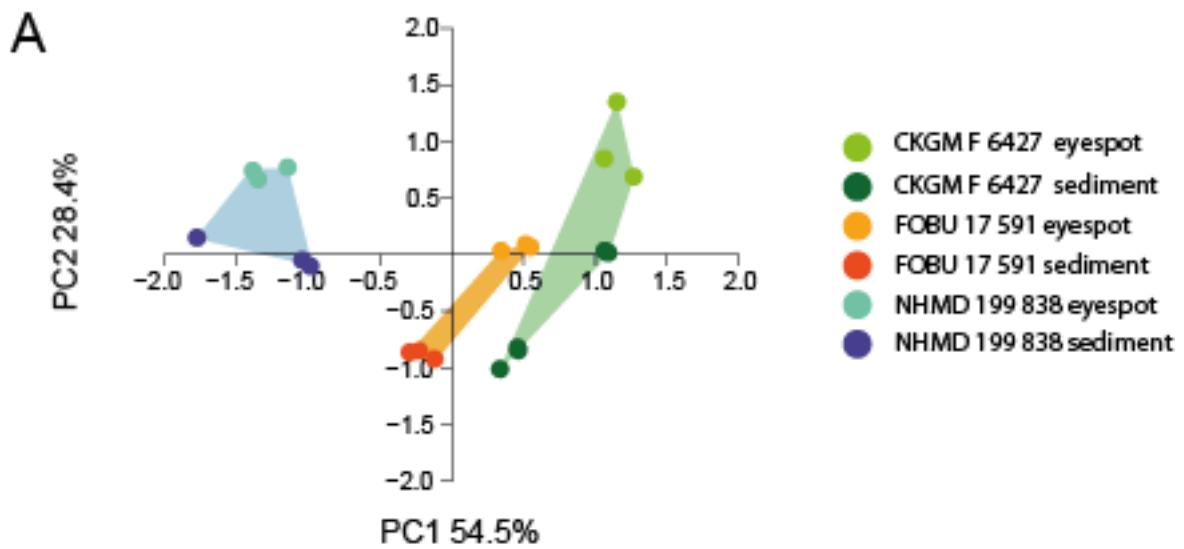
81

82 **Fig. S8.** MCA spectra from regions of interest in SRS-XRF maps of fossil eyespots of *D. macrurus*,

83 NHMD 199838 (*Tetrodontiformes indet.*) and UGF 2015-16 X-axis, X-ray emission energy (keV). Y-

84 axis, counts. Yellow line denotes measured data; green line denotes the computed fit.

85



86
 87 **Fig. S9.** A, principal Components Analysis of chemical data for fossil melanosomes from CKGM F
 88 6427 (*Dapalis macrurus*), FOBU 17 591 (*Knightsia*) and NHMD 199 838 (Tetradontiformes indet.). B,
 89 Biplot of key elements and their contribution to variation in A. The analyses used data for Ca, Fe,
 90 Cu and Zn only.

91
 92
 93
 94
 95
 96
 97
 98
 99
 100
 101

102

103

104 **Table S1.** List of maturation treatments.

Melanosome extracts	Experimental maturation treatment
A-C	Unmatured
D-E	Matured in DD water, with elevated temperature only
F-G	Matured in DD water, with elevated temperature and pressure
H-J	Matured in Zn, with elevated temperature and pressure
K-L	Matured in Cu and Zn, with elevated temperature and pressure
M-N	Matured in Cu, with elevated temperature only
O-P	Matured in Cu, with elevated temperature and pressure

105

106

107 **Table S2.** Statistical analyses of trace element concentrations in melanosome extracts. A, ANOVA /
 108 Welch's F-test (*); B, Kruskal-Wallis; C, Post-hoc analyses for Welch F test and Kruskal-Wallis
 109 (Dunn's post hoc). Cu T only, extract with added Cu-rich solution treated to elevated temperature; Cu
 110 T&P, extract with added Cu-rich solution treated to elevated temperature and pressure; Cu & Zn,
 111 extract with added Cu-and Zn-rich solution treated to elevated temperature and pressure; DD T only,
 112 extract with added distilled water treated to elevated temperature; DD T&P, extract with added
 113 distilled water treated to elevated temperature and pressure; Zn, extract with added Zn-rich solution
 114 treated t elevated temperature and pressure; UNMAT, untreated melanosomes. † indicates
 115 concentration data that were log-transformed prior to statistical testing to make the data conform to
 116 normality.

117

A

Element concentration	df	F	p
Fe	2.115 [†]	17.5 [†]	0.1034 [†]
Ca	16.18* [†]	73.39* [†]	7.91 E-11* [†]
Cu	17.47* [†]	118.8* [†]	5.792 E-13* [†]

118

B

Element concentration	H (chi ²)	p
Zn	23.33	0.000693

119

C

	UNMAT	DD T only	DD T & P	Zn	Cu & Zn	Cu T & P	Cu T only
Ca	UNMAT	2.43E-01	1.57E-01	4.44E-03	1.03E-03	1.23E-01	1.12E-01
	DD T only	2.43E-01	8.21E-01	2.06E-04	4.86E-05	1.34E-02	1.19E-02
	DD T & P	1.57E-01	8.21E-01	7.48E-05	1.80E-05	6.91E-03	6.10E-03
	Zn	4.44E-03	2.06E-04	7.48E-05	4.61E-01	3.17E-01	3.39E-01
	Cu & Zn	1.03E-03	4.86E-05	1.80E-05	4.61E-01	1.12E-01	1.22E-01
	Cu T & P	1.23E-01	1.34E-02	6.91E-03	3.17E-01	1.12E-01	9.67E-01
	Cu T only	1.12E-01	1.19E-02	6.10E-03	3.39E-01	1.22E-01	9.67E-01
Cu	UNMAT	7.07E-01	5.32E-01	6.49E-01	8.75E-04	2.41E-03	1.78E-03
	DD T only	7.07E-01	8.21E-01	4.34E-01	7.21E-04	1.85E-03	1.39E-03
	DD T & P	5.32E-01	8.21E-01	3.02E-01	3.08E-04	8.37E-04	6.20E-04
	Zn	6.49E-01	4.34E-01	3.02E-01	3.49E-03	8.60E-03	6.57E-03
	Cu & Zn	8.75E-04	7.21E-04	3.08E-04	3.49E-03	7.89E-01	8.53E-01
	Cu T & P	2.41E-03	1.85E-03	8.37E-04	8.60E-03	7.89E-01	9.34E-01
	Cu T only	1.78E-03	1.39E-03	6.20E-04	6.57E-03	8.53E-01	9.34E-01
	UNMAT	DD T only	DD T & P	Zn	Cu & Zn	Cu T & P	Cu T only

	UNMAT		7.68E-01	1.75E-01	6.19E-03	1.79E-03	1.79E-03	5.61E-03
	DD T only	7.68E-01		8.10E-01	1.12E-01	9.27E-02	6.56E-02	6.56E-02
	DD T & P	1.75E-01	8.10E-01		8.75E-02	5.08E-03	8.24E-03	3.06E-02
Zn	Zn	6.19E-03	1.12E-01	8.75E-02		6.80E-01	5.96E-01	2.16E-01
	Cu & Zn	1.79E-03	9.27E-02	5.08E-03	6.80E-01		9.36E-01	4.71E-01
	Cu T & P	1.79E-03	6.56E-02	8.24E-03	5.96E-01	9.36E-01		4.71E-01
	Cu T only	5.61E-03	6.56E-02	3.06E-02	2.16E-01	4.71E-01	4.71E-01	

119

120

121

122

123

124

125

126 **Table S3.** Statistical analyses of trace element concentrations in fossil eyespots. A, Welch's ANOVA;
 127 B, Kruskal-Wallis test; C, Dunn's post hoc analyses for both Welch's ANOVA and Kruskal-Wallis. †
 128 indicates concentration data that were log-transformed prior to statistical testing due to non-normality.

A

Element concentration	df	F	p
Ca	2.668	37.62	0.01109
Fe	8 [†]	162 [†]	0.03136 [†]
Cu	2.983 [†]	13.7 [†]	0.8371 [†]

129

B

Element concentration	H (chi ²)	p
Zn	0.3556	0.8371

130

C

		CKGM F 6327	FOBU 17 591	NHMD 199838
Ca	CKGM F 6327		0.8815	0.05263
	FOBU 17 591	0.8815		0.03689
	NHMD 199838	0.05263	0.03689	
Fe	CKGM F 6327		0.8815	0.03689
	FOBU 17 591	0.8815		0.05263
	NHMD 199838	0.03689	0.05263	
Cu	CKGM F 6327		0.1797	0.00729
	FOBU 17 591	0.1797		0.1797
	NHMD 199838	0.00729	0.1797	

131

132

133

134 **Table S4.** Statistical analyses of trace element concentrations between fossil eyespots and associated
 135 sedimentary matrix. A, t-test; B, Welch's F-test; C, Mann Whitney-U. † indicates concentration data
 136 that were log-transformed prior to statistical testing due to non-normality.

137

A

Element concentration	Specimen	df	t	p
Ca	CKGM F 6327	6	3.9178	0.0078
	FOBU 17 591	4	0.0813	0.93913
Fe	CKGM F 6327 †	6†	3.2465†	0.0228†
Cu	NHMD 199838†	4†	7.0917†	0.0020877†
	FOBU 17 591	4	0.0308	0.96693
Zn	NHMD 199838	4	1.454	0.21963

B

Element concentration	Specimen	df	F	p
Ca	NHMD 199838	2.043	3.073	0.219
	FOBU 17 591	2.07	106	0.008268
Fe	NHMD 199838	2.062	0.6704	0.4967
	CKGM F 6327†	2.004†	2.07†	0.01327†
Cu	FOBU 17 591	2.07	0.0813	0.93913

C

Element concentration	Specimen	df	U	p
Zn	CKGM F 6327	1875, 2.625	6	0.21963

138

139

140

141

142

143 **Table S5.** Statistical analyses of differences between the trace element concentrations in unmaturred
 144 melanosome extracts and fossils. A, ANOVA; B, Kruskal-Wallis. † indicates concentration data that
 145 were log-transformed prior to statistical testing due to non-normality.

A

Element concentration	df	F	p
Fe	17†	3.478†	0.08063†

B

Element concentration	H (chi ²)	p
Ca	1.421	0.2332
Cu	0.001949	0.9648
Zn	12.79	0.000349

146

147